

OPEN ACCESS

Evaluation of the Efficiency of an Elevated Temperature Proton Exchange Membrane Water Electrolysis System

To cite this article: Marco Bonanno *et al* 2021 *J. Electrochem. Soc.* **168** 094504

View the [article online](#) for updates and enhancements.



ECS Membership = Connection

ECS membership connects you to the electrochemical community:

- Facilitate your research and discovery through ECS meetings which convene scientists from around the world;
- Access professional support through your lifetime career;
- Open up mentorship opportunities across the stages of your career;
- Build relationships that nurture partnership, teamwork—and success!

Join ECS!

Visit electrochem.org/join





Evaluation of the Efficiency of an Elevated Temperature Proton Exchange Membrane Water Electrolysis System

Marco Bonanno,^{1,2} Karsten Müller,³ Boris Bensmann,⁴ Richard Hanke-Rauschenbach,⁴ Retha Peach,¹ and Simon Thiele^{1,2,z}

¹Forschungszentrum Jülich GmbH, Helmholtz-Institute Erlangen-Nuremberg for Renewable Energy (IEK-11), 91058 Erlangen, Germany

²Department for Chemical and Biological Engineering, Friedrich-Alexander University Erlangen-Nuremberg, 91058 Erlangen, Germany

³Institute for Technical Thermodynamics, University of Rostock, 18059 Rostock, Germany

⁴Institute of Electric Power Systems, Leibniz University Hannover, 30167 Hannover, Germany

In recent years, a significant interest has been growing in elevated temperature (ET) electrolytes for proton exchange membrane water electrolysis (PEMWE). In this study, the energy and exergy analysis developed for PEMWE has been extended to evaluate the performance of ET-PEMWE, with the model aiming to utilise the energy in the most efficient manner and also take into account potential heat losses. The latter is particularly important considering that heat losses become more pronounced with higher temperature differences. The model shows that the stack operates in autothermic mode over a considerable range of current density. Thus heating inputs to the stack and feed water become progressively unnecessary as polarization losses make up for these heating requirements. This also allows surplus heat to be utilised for secondary applications. The exergy efficiency for ET has been calculated to surpass that for low temperature (LT), with the maximum improvement reaching 3.8% points. Taking into account exergy favours higher temperature differences—a benefit which outweighs the fact that a greater quantity of thermal power is recovered in the LT system (due to higher polarization losses). This finding also shows the suitability of adopting exergy efficiency as the performance indicator for PEMWE systems.

© 2021 The Author(s). Published on behalf of The Electrochemical Society by IOP Publishing Limited. This is an open access article distributed under the terms of the Creative Commons Attribution Non-Commercial No Derivatives 4.0 License (CC BY-NC-ND, <http://creativecommons.org/licenses/by-nc-nd/4.0/>), which permits non-commercial reuse, distribution, and reproduction in any medium, provided the original work is not changed in any way and is properly cited. For permission for commercial reuse, please email: permissions@iopublishing.org. [DOI: [10.1149/1945-7111/ac2188](https://doi.org/10.1149/1945-7111/ac2188)]



Manuscript submitted May 26, 2021; revised manuscript received July 16, 2021. Published September 20, 2021.

Supplementary material for this article is available [online](#)

List of Symbols

Latin Letters

a	activity, —
A_{MEA}	membrane electrode assembly area, m^2
A_{stack}	stack outside surface area, m^2
B	second virial coefficient, $m^3 mol^{-1}$
c_p	specific heat capacity, $J mol^{-1} K^{-1}$
E	exergy of substance, $J mol^{-1}$
\dot{E}	rate of exergy input, W
f	fugacity, Pa
G	molar Gibbs Free Energy, $J mol^{-1}$
h_c	convective heat transfer coefficient, $W m^{-2} K^{-1}$
h_r	radiative heat transfer coefficient, $W m^{-2} K^{-1}$
H	molar enthalpy, $J mol^{-1}$
i	electrical current density, $A m^{-2}$
I	electrical current, A
k	thermal conductivity, $W m^{-1} K^{-1}$
\dot{N}	molar flow, $mol s^{-1}$
p	pressure, Pa
$P_{electric}$	electrical power, W
$\dot{q}_{loss,pipe}$	heat losses per metre length of pipework, $W m^{-1}$
\dot{Q}	molar thermal energy demand, $J mol^{-1}$
\dot{Q}	heat energy exchange rate, W
\dot{Q}_{heat,H_2O}	thermal power input to the feed water via heat exchanger, W
$\dot{Q}_{loss,pipe}$	thermal losses from pipework, W
$\dot{Q}_{loss,stack}$	thermal losses from stack, W
\dot{Q}_{max}	theoretical maximum heat exchanger rate between two fluid streams, W
\dot{Q}_{react}	thermal power demand for water electrolysis reaction to occur, W

\dot{Q}_{stack}	thermal power supplied to/emanating from the stack, W
$\dot{Q}_{theo,heat,H_2O}$	minimum rate of thermal energy input to the feed water, W
\dot{Q}_J	thermal power arising from polarization losses, W
\dot{Q}_{heat,H_2O}	thermal power input to feed water following energy recovery, W
$\dot{Q}_{heat,H_2O,rec}$	recovered thermal power available for feed water heating (partial recovery), W
$\dot{Q}_{stack,heat}$	recovered thermal power to fully provide for feed water heating, W
$\dot{Q}_{stack,rec}$	recovered thermal power available for secondary heating application, W
r	radius, m
R_{th}	thermal resistance, $m^2 K W^{-1}$
$R_{th,T}$	total thermal resistance for combined modes of heat transfer, $m^2 K W^{-1}$
$R'_{th,T}$	total thermal resistance per unit length of pipework, $m K W^{-1}$
S	molar entropy, $J mol^{-1} K^{-1}$
t	thickness, m
T	temperature, K
T_s	external heat source temperature, K
T_e	ambient/environment temperature, K
T_m	mean temperature of the stack surface, K
U	voltage, V
\tilde{V}	molar volume, $m^3 mol^{-1}$
Z	dimensionless compressibility factor, —
Subscripts	
0	in standard ambient conditions
act	activation
an	anode
cat	cathode
chem	chemical
cond	conduction

^zE-mail: si.thiele@fz-juelich.de

<i>conv</i>	convection
<i>e</i>	environment
<i>electric</i>	electrical
<i>en</i>	energy
<i>ex</i>	exergy
<i>heat, H₂O</i>	water heating
<i>inner</i>	inner
<i>ins</i>	insulation
<i>mass</i>	mass transfer
<i>max</i>	maximum
<i>ohm</i>	ohmic
<i>out</i>	outlet
<i>outer</i>	outer
<i>pipe</i>	pipework
<i>rad</i>	radiation
<i>react</i>	reacting
<i>rec</i>	recovered
<i>ref</i>	reference
<i>rev</i>	reversible
<i>sat</i>	saturated
<i>stack</i>	stack
<i>th</i>	thermal
<i>theo</i>	theoretical
<i>therm</i>	thermomechanical
<i>T</i>	total
Superscripts	
<i>T</i>	at stack temperature <i>T</i>
<i>T₀</i>	at temperature <i>T₀</i>
*	standard pressure and generic temperature
Greek Letters	
γ	specific heat production due to internal dissipations, J mol ⁻¹
ε	effectiveness factor, –
ϵ	emittance, 0.6
η	efficiency, –
σ	Stefan-Boltzmann constant, 5.67×10^{-8} W m ⁻² K ⁻⁴
ϕ	fugacity coefficient, –
ΔG	molar Gibbs free energy variation, J mol ⁻¹
ΔH	molar enthalpy variation, J mol ⁻¹
ΔS	molar entropy variation, J mol ⁻¹ K ⁻¹
Constants	
<i>E_{chem}</i>	chemical exergy content of Hydrogen, 236 kJ mol ⁻¹
<i>F</i>	Faraday constant, 96,485 C mol ⁻¹
<i>LHV_{H₂}</i>	molar lower heating value of hydrogen, 242 kJ mol ⁻¹
<i>R</i>	universal constant of gases, 8.314 J mol ⁻¹ K ⁻¹

Growing energy demands and socio-economic concerns are pushing for decarbonisation of energy sources.¹ Such a transition is however hampered by the intermittent nature of some renewables such as solar and wind energy. Hydrogen as an energy carrier is therefore viewed as an alternative to mitigate this issue. Amongst the different technologies for hydrogen production, Proton Exchange Membrane Water Electrolysis (PEMWE) has received considerable attention mainly due to the high-intensity and flexibility of the process, its compact and modular design and high product purity.²

Elevated Temperature (ET) PEMWE

PEMWE has been typically operated at temperatures in the region of 60 °C–80 °C. In recent years, however, a significant interest has been addressed to the development of higher temperature (>100 °C) polymer electrolytes. Such efforts potentially could be rewarded with a number of advantages, mainly improvement in electrode kinetics, reduction in overpotentials³ and a lower reversible potential—which translate into a lower threshold of minimum electrical work.⁴ Moreover, increasing the operation temperature is

seen as a promising way towards reduction of electrocatalyst loading utilised in low temperature (LT) PEMWE,² together with improved heat recovery due to the higher temperature differences.⁵

Studies involving higher temperatures have either operated the electrolyser with steam^{3,6–9} or with liquid water by pressurizing the cell, causing an increase in the saturated vapour temperature and hence delaying the change of state from liquid to gas.^{2,10–15}

In liquid based systems, perfluorosulfonic acid (PFSA) type membranes were mainly studied and operate in a temperature range between 110 °C and 150 °C.^{2,10–15} On the other hand, phosphoric-acid doped based membranes were mainly adopted for steam systems. In this case, the operating temperature typically corresponded to 130 °C,^{3,6,7} with one study recording data at temperatures as high as 170 °C.⁸

Modelling PEMWE systems.—Mathematical modelling may be employed to assess the performance of a system from multiple perspectives. In their review of electrolysis systems' modelling, Olivier et al.¹⁶ included also thermal modelling to capture the behaviour and influence of temperature on the cell or stack.

Moreover, efficiency is one of the central performance indicators for hydrogen production systems. Multiple studies have used such a benchmark analysis to compare hybrid systems involving PEMWE, such as the inclusion of a gas turbine or renewable energy systems.^{17–23} Whilst these do not make any reference to the heat management of the electrolysis stack, other studies specifically focus on understanding the effect of waste heat utilization in PEMWE systems.^{24,25} Such an approach was also adopted for Solid Oxide Steam Electrolysis (SOEC).^{26,27}

Except in the case of Moradi Nafchi et al.²¹ and SOEC systems, the operating temperature in these studies has been limited to 80 °C. (Moradi Nafchi et al. simulate the performance of a high temperature (170 °C) PEM electrolyzer, but the model focuses on the integration of PEMWE to a concentrating solar power plant).

In this study, the energy and exergy analysis developed for PEMWE has been further extended to investigate the thermodynamic performance of an ET system (at 120 °C) involving liquid water and based on a PFSA type membrane. The model takes into account heat losses since it would be expected that these become more pronounced with higher temperatures. Moreover, in view that higher temperature differences facilitate energy recovery, the model considers a configuration capable of utilising waste energy. The results are also compared to typical efficiencies in the LT operating regime. This study furthers the understanding of the expected performance with ET-PEMWE systems.

Theory and Model Description

An ET-PEMWE system for hydrogen production.—Figure 1 displays the schematic for a possible configuration when operating ET-PEMWE. The system is operated with liquid water and hence needs to be kept under pressure to ensure that phase change does not occur. The electrochemical reaction for hydrogen production occurs in the stack, to which water at the required temperature is fed, together with electrical energy and, if necessary, heat. The generated gases are separated and the residual water flow re-circulated. (For simplicity, the schematic only considers water being fed into one compartment). Some of the water is consumed in the reaction and water hence needs to be dosed into the loop. This makeup water (input at room temperature) is heated to the operating temperature by the *Heat Exchanger 1*, which must also provide energy for the heat losses within the pipework. *Heat Exchanger 2* allows potential energy recovery from the stack to the dosing water stream.

Thermodynamic analysis of ET-PEMWE.—The theoretical energy required for hydrogen production $\Delta H_{stack}(T, p)$ from water electrolysis is the sum of thermal energy demand $\Delta Q_{rev}(T, p)$ and electrical energy demand $\Delta G_{stack}(T, p)$, i.e.,

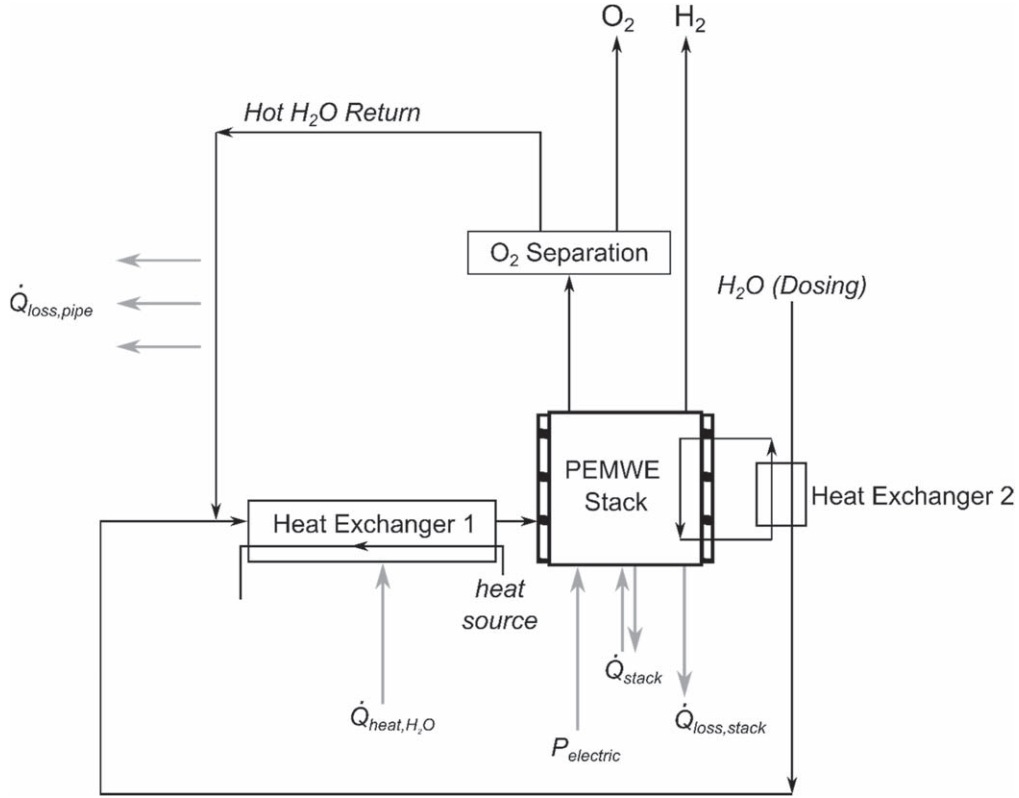


Figure 1. Schematic of an ET-PEMWE setup utilising recirculating liquid water.

$$\Delta H_{stack}(T, p) = \Delta G_{stack}(T, p) + \Delta Q_{rev}(T, p) \quad [1]$$

Where T is the stack temperature, p refers to pressure and $\Delta G_{stack}(T, p)$ is the change in the Gibbs free energy which gives rise to a minimum voltage supply for the electrochemical reaction to occur, termed as the reversible potential U_{rev} . Moreover, $\Delta Q_{rev}(T, p) = T\Delta S(T, p)$ and represents the thermal energy component which must be provided in addition to this minimum voltage supply. ΔG_{stack} can hence be calculated based on the temperature-dependent values of enthalpy (H) and entropy (S) for O_2 and H_2 which can be found in data tables, such as in O'Hayre et al.²⁸ whilst corresponding parameters for H_2O (in liquid state above 100 °C) can be extracted from the National Institute of Standards and Technology (NIST) online WebBook.²⁹

The effect of irreversible losses in the stack.—The rate of electrical energy input, $P_{electric}$ to the stack is given by:

$$P_{electric} = U \cdot I \quad [2]$$

Where U is the applied voltage and I refers to the operating current from which, assuming a current utilization of 100%, allows the calculation of hydrogen production rate ($\dot{N}_{H_2,out}$):

$$\dot{N}_{H_2,out} = \frac{I}{2F} = \frac{iA_{MEA}}{2F} \quad [3]$$

Where i is the current density, A_{MEA} is the membrane electrode assembly area and F is the Faraday constant (96,485 C mol⁻¹).

Considering that the $\Delta Q_{rev}(T, p)$ component can be provided as heat, $P_{electric}$ from Eq. 2 can also be written as:

$$P_{electric} = (\Delta G_{stack}(T, p) + \gamma) \cdot \dot{N}_{H_2,out} \quad [4]$$

Where γ is an entropy generation term associated with irreversibility arising from charge transfer, proton and electronic resistance and mass transport:

$$\gamma = 2F(U_{act} + U_{ohm} + U_{mass}) \quad [5]$$

Where U_{act} , U_{ohm} , U_{mass} respectively refer to the activation, ohmic and mass transport overpotentials.

These overvoltages contribute to heat production (termed as Joule heating) and can be quantified based on the difference between the applied cell voltage (as observed from a polarization curve, for instance) and the minimum voltage supply for the electrochemical reaction to occur:

$$\dot{Q}_J = I(U - U_{rev}) \quad [6]$$

Where U_{rev} refers to the reversible potential deduced from:

$$U_{rev} = -\frac{\Delta G_{rev}^*(T)}{2F} \quad [7]$$

Where $\Delta G_{rev}^*(T)$ refers to the Gibbs free energy change at a reference pressure and can be calculated as a function of temperature by using the respective enthalpy and entropy data in Eq. 1. The Gibbs free energy change can be further corrected for non-standard pressure conditions from Ref. 30:

$$\Delta G_{rev}(T, p) = \Delta G_{rev}^*(T) + RT \ln \left(\frac{a_{H_2} a_{O_2}^{1/2}}{a_{H_2O}} \right) \quad [8]$$

Where R is the universal constant of gases and a is the activity. Whilst the activity of water is considered as one, that of hydrogen and oxygen can be expressed as:

$$a_i = \frac{f_i}{P_{ref}} \quad [9]$$

Where P_{ref} refers to the reference pressure at which the value of $\Delta G_{rev}^*(T)$ is taken and f_i is the fugacity to account for the departure of the products from ideal gas behaviour, derived using the Virial equation of State:³¹

$$Z = \frac{p\tilde{V}}{RT} = 1 + \frac{B(T)}{\tilde{V}} + \frac{C(T)}{\tilde{V}^2} + \dots \quad [10]$$

Where Z refers to a dimensionless compressibility factor, \tilde{V} refers to the molar volume and $B(T)$ and $C(T)$ are respectively the second and third virial coefficients. It suffices to solely consider the second virial coefficient for pressures up to 15 bar.³¹ Complete details for deriving the fugacity are provided in the appendix.

Having calculated $\Delta G_{rev}(T, p)$, Eq. 7 can hence yield the reversible potential at the non-standard temperature and pressure by replacing $\Delta G_{rev}^*(T)$ with $\Delta G_{rev}(T, p)$.

Thermal energy in the stack.—Thermal power would therefore need to be supplied to or emanating from the stack (\dot{Q}_{stack}), depending on the amount of power required to sustain the reaction ($T\Delta S$ component, hereunder referred to as \dot{Q}_{react}) and the heat losses originating both due to the irreversibility (\dot{Q}_J) and also due to the temperature difference between the stack and its environment:

$$\dot{Q}_{stack} = (\dot{Q}_{react} + \dot{Q}_{loss,stack} - \dot{Q}_J) \quad [11]$$

Where \dot{Q}_{react} refers to the $T\Delta S$ heat component in Eq. 1. $\dot{Q}_{loss,stack}$ refers to the thermal losses from the stack and assuming that the entire stack has the same temperature as that of the reaction, can be quantified from:

$$\dot{Q}_{loss,stack} = \frac{1}{R_{th,T}} A_{stack} (T_{stack} - T_e) \quad [12]$$

And where A_{stack} is the outside surface area of the stack, T_{stack} is the stack operating temperature, T_e is the temperature of the surrounding environment and $R_{th,T}$ refers to the total thermal resistance, capturing the combined modes of heat transfer involving conduction through the insulation and both convection and radiation on the outer surface, schematically shown in Fig. 2 and computed from Refs. 32, 33:

$$R_{th,T} = \frac{1}{h_c + h_r} + \frac{t_{stack,ins}}{k_{stack,ins}} \quad [13]$$

Where $t_{stack,ins}$ is the insulation thickness, $k_{stack,ins}$ refers to the conductivity of the insulation and h_c and h_r respectively refer to the convective and radiative heat transfer coefficients. The latter parameter can be approximated from Ref. 33:

$$h_r = 4\epsilon\sigma T_m^3 \quad [14]$$

Where ϵ refers to the emittance of the stacks' outside material, σ refers to the Stefan-Boltzmann constant and T_m refers to the mean temperature of the stack surface.

If the heat required for \dot{Q}_{react} and $\dot{Q}_{loss,stack}$ is larger than the heat produced within the stack due to the irreversibility (\dot{Q}_J), then additional heat would need to be added to the stack. However, if the opposite is true, then additional heat is not needed but instead can be recovered to heat up the compensatory reactant water entering the system (to make up for the water consumed in the reaction), and cooling the stack in the process.

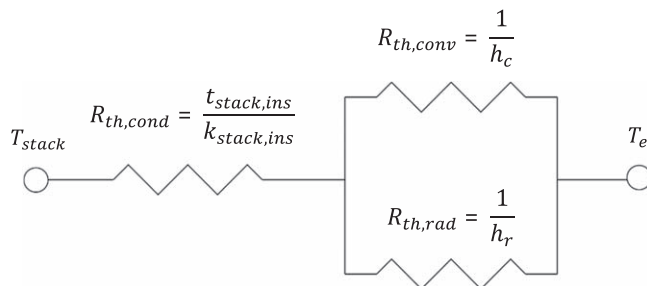


Figure 2. Thermal circuit for heat losses from the stack (adapted from Ref. 33).

Energy and exergy efficiencies as a means of performance indicators.—The performance of the systems concerned can be evaluated in terms of energy efficiency (η_{en}) and exergy efficiency (η_{ex}), defined as:

$$\eta_{en} = \frac{LHV_{H_2} \cdot \dot{N}_{H_2,out}}{P_{electric} + \dot{Q}_{stack} + \dot{Q}_{heat,H_2O}} \quad [15]$$

$$\eta_{ex} = \frac{E_{H_2} \cdot \dot{N}_{H_2,out}}{\dot{E}_{electric} + \dot{E}_{stack} + \dot{E}_{heat,H_2O}} \quad [16]$$

Where LHV_{H_2} is the molar lower heating value of hydrogen, E_{H_2} is the molar exergy content of hydrogen, $\dot{N}_{H_2,out}$ is the outlet flow rate of hydrogen (from Eq. 3), $P_{electric}$ is the actual electrical power input to the PEM electrolyzer (as derived from polarization curves) to provide the $\Delta G_{stack}(T, p)$ component in Eq. 1, \dot{Q}_{heat,H_2O} is the rate of thermal energy input to the heat exchanger for heating up the water and \dot{E} is the corresponding rate of exergy input for the variables in the denominator of Eq. 15. It should be noted that $P_{electric}$ is equal to $\dot{E}_{electric}$ since the exergy associated with electricity is equal to the energy.³⁴

Neglecting the kinetic and potential energies, the exergy of a substance can be obtained:

$$E = E_{chem} + E_{therm} \quad [17]$$

Where E_{chem} is the chemical exergy (due to the specific composition of a component) and E_{therm} is the thermomechanical exergy which results from the deviation of temperature and pressure from the environmental values. The values of E_{chem} can be found in data sheets³⁵ whilst E_{therm} can be determined from the following expression:³⁶

$$E_{therm} = c_p \left(T - T_0 - T_0 \ln \left[\frac{T}{T_0} \right] \right) + RT_0 \ln \left[\frac{P}{P_0} \right] \quad [18]$$

Where T_0 and p_0 respectively refer to the temperature and pressure in standard ambient conditions whilst c_p refers to the specific heat capacity of hydrogen, taken at standard temperature due to its small dependency on temperature.

Feed water heating.—Additional water must be fed to the stack to make up for the consumption in the reaction. This requires thermal energy to be put in (*Heat Exchanger 1* of Fig. 1) to raise its temperature to that in the operating stack.

The actual heat exchange rate (\dot{Q}) between two fluid streams can be determined by:

$$\dot{Q} = \epsilon \dot{Q}_{max} \quad [19]$$

Where ϵ refers to the effectiveness factor (typically in the range of 0.8–0.9 for counter-flow heat exchangers³⁷) and \dot{Q}_{max} is the

theoretical maximum heat exchanger rate between the two fluid streams.

Since the hot liquid water exiting the PEM electrolyzer is recirculated, only the supplemental water needs to be heated by the heat exchanger, as described by Ni et al.²⁵ By also accounting for losses within the pipework, the theoretical heat ($\dot{Q}_{theo,heat,H_2O}$) needed to raise the temperature of the feeding water to that of the PEM electrolyzer can be determined by:

$$\dot{Q}_{theo,heat,H_2O} = \dot{N}_{H_2O,react} (H_{H_2O}^T - H_{H_2O}^{T_0}) + \dot{Q}_{loss,pipe} \quad [20]$$

Where $\dot{N}_{H_2O,react}$ refers to the molar flow of water consumed in the reaction and is numerically equal to $\dot{N}_{H_2,out}$, given by Eq. 3. Moreover, $H_{H_2O}^T$ and $H_{H_2O}^{T_0}$ are enthalpies of liquid water at temperature T and T_0 , respectively and $\dot{Q}_{loss,pipe}$ refers to the heat losses within the pipework, which can be approximated from Ref. 37:

$$\dot{q}_{loss,pipe} = \frac{T - T_0}{R'_{th,T}} \quad [21]$$

Where $\dot{q}_{loss,pipe}$ refers to the heat losses per metre length of pipework and $R'_{th,T}$ refers to the total thermal resistance, which in this case would be dominated by conduction in the insulation and convection and radiation on the surface exposed to air and hence, approximated using:³⁷

$$R'_{th,T} = \frac{\ln\left(\frac{r_{outer}}{r_{inner}}\right)}{2\pi k_{pipe,ins}} + \frac{1}{2\pi r_{outer} h_c + 2\pi r_{outer} h_r} \quad [22]$$

Where r_{outer} and r_{inner} respectively refer to the outer and inner radius of the insulation (covering the pipework) and $k_{pipe,ins}$ refers to thermal conductivity of the pipework insulation. This can be realistically deduced by following typical insulation conductivities suggested by ASHRAE guidelines³⁸ typically adopted in industry. Moreover, h_c refers to the convection heat transfer coefficient. Free convection of gases typically involves values between 5 and 25 W m⁻² K⁻¹. This simple thermal model for the pipework assumes one-dimensional heat transfer in radial direction and negligible tube wall thermal resistance.

Thus, following Eq. 19, the rate of heat input (\dot{Q}_{heat,H_2O}) via the heat exchanger for further heating up the water stream can be determined by:

$$\varepsilon \dot{Q}_{heat,H_2O} = \dot{Q}_{theo,heat,H_2O} \quad [23]$$

Additional considerations.—A number of simplifications should be highlighted. The enthalpy of the gaseous outlet streams is not recovered. Moreover, the pumps need work as input. These are both not accounted for since it is expected that the respective energy share would only have a minor effect on the efficiency calculation.³⁹ The validity of the assumption with regards to the gas streams is further discussed in the *Results and Discussion* section.

Heat management configurations.—As outlined above, the interplay between heat supply and recovery in the stack calls for the study of different scenarios. The energy and exergy definitions would in turn need to cater for the specific arrangement, hereunder following that put forward by Zhang et al.²⁷

Case 1: $\dot{Q}_{stack} > 0$.—Additional heat energy needs to be supplied in case \dot{Q}_J is not sufficient to make up for the $T\Delta S$ component and stack losses. In this case, the two efficiencies can be calculated as:

$$\eta_{en} = \frac{LHV_{H_2} \cdot \dot{N}_{H_2,out}}{P_{electric} + \dot{Q}_{stack} + \dot{Q}_{heat,H_2O}} \quad [24]$$

$$\eta_{ex} = \frac{E_{H_2} \cdot \dot{N}_{H_2,out}}{P_{electric} + \dot{Q}_{stack} \left(1 - \frac{T_0}{T_s}\right) + \dot{Q}_{heat,H_2O} \left(1 - \frac{T_0}{T_s}\right)} \quad [25]$$

Where T_s refers to the temperature of the external heat source.

The key energy components of *Case 1* with respect to the general schematic presented earlier (as Fig. 1) are highlighted in Fig. 3a.

Case 2: $\dot{Q}_{stack} = 0$ (i.e. *autothermal operation*).—When the heat produced inside the stack equals the heat required, it is not necessary to supply heat to the electrolysis stack from the external heat source since the electrochemical reaction becomes self-sustaining. In this case, the efficiencies would correspond to:

$$\eta_{en} = \frac{LHV_{H_2} \cdot \dot{N}_{H_2,out}}{P_{electric} + \dot{Q}_{heat,H_2O}} \quad [26]$$

$$\eta_{ex} = \frac{E_{H_2} \cdot \dot{N}_{H_2,out}}{P_{electric} + \dot{Q}_{heat,H_2O} \left(1 - \frac{T_0}{T_s}\right)} \quad [27]$$

The key energy components of *Case 2* are highlighted in Fig. 3b.

Case 3: $\dot{Q}_{stack} < 0$.—In this case, surplus heat is available in the stack and may be used to heat the feed water through an additional heat exchanger (*Heat Exchanger 2* in Fig. 1). The performance of the system also depends on whether the surplus energy in the stack would be sufficient to heat the compensatory feed water or not, calling for a distinction within *Case 3*.

Case 3A: $\dot{Q}_{heat,H_2O} \left(1 - \frac{T_0}{T_s}\right) > |\dot{Q}_{stack} \left(1 - \frac{T_0}{T}\right)|$.—The surplus heat from the stack may only partly heat the compensatory feed water. By expressing this additional heat energy in terms of the external heat source connected to *Heat Exchanger 1*:

$$\dot{Q}_{heat,H_2O,rec} = |\dot{Q}_{stack}| \left(1 - \frac{T_0}{T}\right) \frac{T_s}{(T_s - T_0)} \quad [28]$$

With $\dot{Q}_{heat,H_2O,rec}$ representing the heat transferred to the dosing water.

The heat supplied by the external heat source may hence be reduced from \dot{Q}_{heat,H_2O} to $\dot{Q}_{heat,H_2O} - |\dot{Q}_{stack}| \left(1 - \frac{T_0}{T}\right) \left(\frac{T_s}{T_s - T_0}\right)$, hereunder referred to as \dot{Q}'_{heat,H_2O} . The efficiencies can hence be described by:

$$\eta_{en} = \frac{LHV_{H_2} \cdot \dot{N}_{H_2,out}}{P_{electric} + \left(\dot{Q}_{heat,H_2O} - |\dot{Q}_{stack}| \left(1 - \frac{T_0}{T}\right) \left(\frac{T_s}{T_s - T_0}\right)\right)} \quad [29]$$

$$\eta_{ex} = \frac{E_{H_2} \cdot \dot{N}_{H_2,out}}{P_{electric} + \left(\dot{Q}_{heat,H_2O} - |\dot{Q}_{stack}| \left(1 - \frac{T_0}{T}\right) \left(\frac{T_s}{T_s - T_0}\right)\right) \left(1 - \frac{T_0}{T_s}\right)} \quad [30]$$

The key energy components of *Case 3A* are highlighted in Fig. 3c.

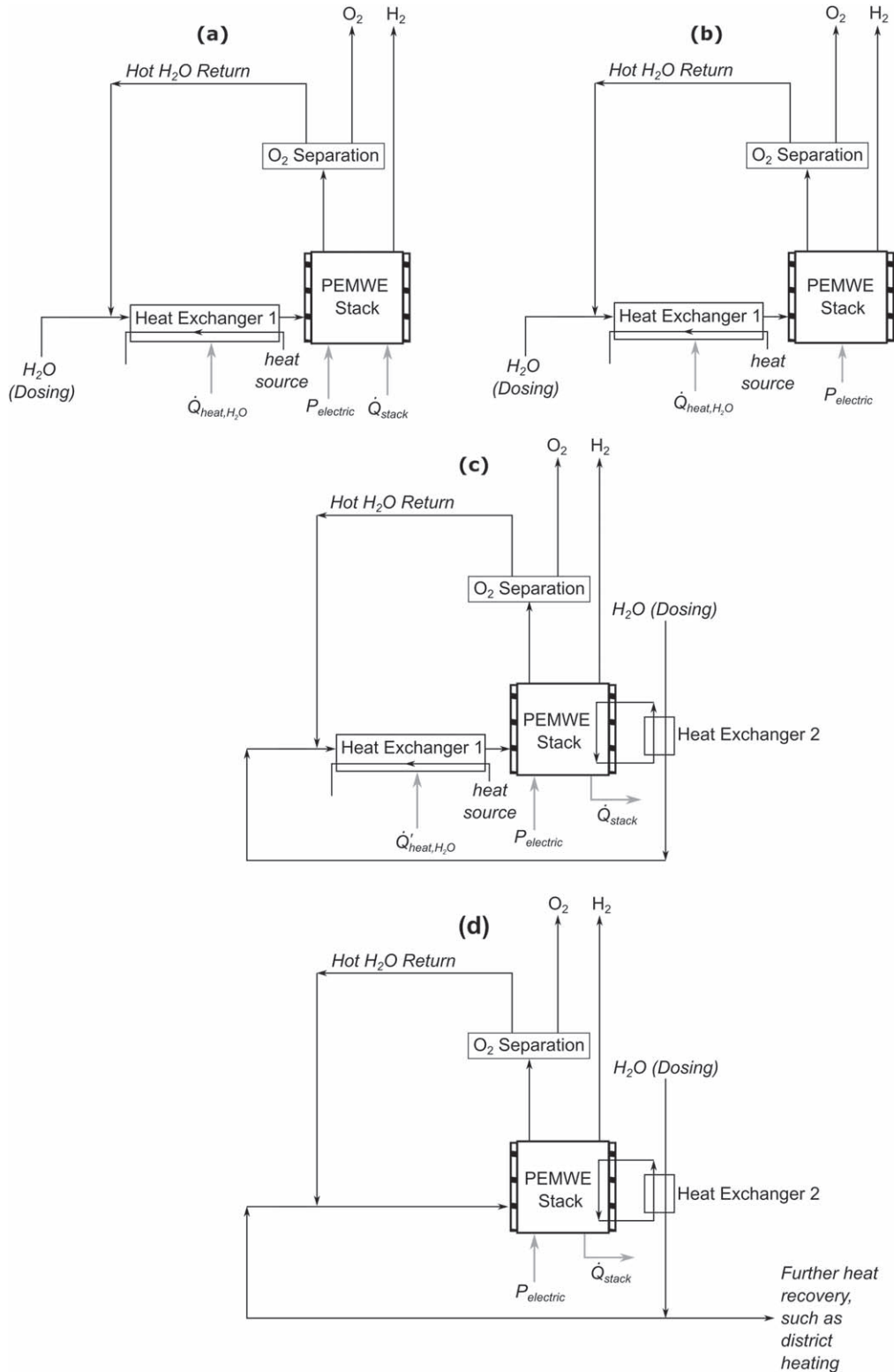


Figure 3. Heat management strategies for an ET-PEMWE setup corresponding to (a) Case 1, (b) Case 2, (c) Case 3 A and (d) Case 3B. Heat losses are omitted since these are contained within other terms in the diagrams.

Case 3B: $\dot{Q}_{heat,H_2O} \left(1 - \frac{T_0}{T_s}\right) \leq \left| \dot{Q}_{stack} \left(1 - \frac{T_0}{T}\right) \right|$ —When $\dot{Q}_{heat,H_2O} \left(1 - \frac{T_0}{T_s}\right) = \left| \dot{Q}_{stack} \left(1 - \frac{T_0}{T}\right) \right|$, the redundant heat from the stack is just sufficient to replace the heat \dot{Q}_{heat,H_2O} supplied by

the external heat source (to bring the water to the required operating temperature). In such case, \dot{Q}'_{heat,H_2O} is driven to 0 W and given no additional heat is needed to be supplied to the feed water, the energy and exergy efficiencies of a water electrolysis system simplify to the following form:

$$\eta_{en} = \frac{LHV_{H_2} \cdot \dot{N}_{H_2,out}}{P_{electric}} \quad [31]$$

$$\eta_{ex} = \frac{E_{H_2} \cdot \dot{N}_{H_2,out}}{P_{electric}} \quad [32]$$

Moreover, when $\dot{Q}_{heat,H_2O} \left(1 - \frac{T_0}{T_s}\right) < \left| \dot{Q}_{stack} \left(1 - \frac{T_0}{T}\right) \right|$, one part of the surplus heat from $|\dot{Q}_{stack}|$ may be used to fully provide the required heat \dot{Q}_{heat,H_2O} whilst the other part of $|\dot{Q}_{stack}|$ can be utilised for a secondary heating application (rather than be simply released to the environment). By taking into account the temperature level of the external heat source in *Heat Exchanger 1*, the portion of heat which needs to be extracted from \dot{Q}_{stack} would in this case correspond to:

$$\dot{Q}_{stack,heat} = \dot{Q}_{heat,H_2O} \left(1 - \frac{T_0}{T_s}\right) \frac{T}{(T - T_0)} \quad [33]$$

Hence, the heat available for secondary applications, $\dot{Q}_{stack,rec}$ would be equal to the remaining heat after the system requirements would have been satisfied and can be expressed as:

$$\dot{Q}_{stack,rec} = |\dot{Q}_{stack}| - \dot{Q}_{stack,heat} \quad [34]$$

For *Case 3B*, Eqs. 31 and 32 would therefore need to be updated to reflect the potential utilisation of the extra heat:

$$\eta_{en} = \frac{LHV_{H_2} \cdot \dot{N}_{H_2,out} + \dot{Q}_{stack,rec}}{P_{electric}} \quad [35]$$

$$\eta_{ex} = \frac{E_{H_2} \cdot \dot{N}_{H_2,out} + \dot{Q}_{stack,rec} \left(1 - \frac{T_0}{T}\right)}{P_{electric}} \quad [36]$$

The key energy components of *Case 3B* are highlighted in Fig. 3d, whereby one portion of the flow exiting *Heat Exchanger 2* is channelled to the stack whilst the other may be used for a secondary use such as space heating, for instance.

The outlined equations together with the respective applicability for the different cases are summarised in Tables I and II.

Model data and implementation.—Polarization curve data.—

The electrical energy input to the stack can be directly extracted from polarization curves. Garbe et al.⁴⁰ provide the experimental performance for the same ET conditions considered for the model (120 °C and 3 bar absolute pressure in the liquid phase). The results for the 50 μm Nafion® NR212 membrane were hence chosen as the

basis for the provision of $P_{electric}$ in the efficiency equations. The stack(s) are considered to collectively house 1 m² of Membrane Electrode Assembly (MEA) area. Table III summarises the key operating parameters for the model.

Data for heat losses' computation.—A typical industrial stack having an MEA size of 1,000 cm² translates in an external surface area of approximately 0.75 m².³² A proportional estimate based on chosen MEA area for this model (1 m²) was hence adopted to roughly compute the surface area required to house the MEAs.

Moreover, the convective heat transfer coefficient (h_c) was taken as 15 W m⁻² K⁻¹.³⁷ This falls under typical values for natural convection, as would be the case for a stack. In the case of the radiative heat transfer coefficient (h_r), a surface emissivity equal to 0.6 was considered. The stack is taken to be insulated with 2 cm thickness of rockwool, having thermal conductivity of 0.045 W m⁻¹ K⁻¹.

With regards to pipework losses, a flow rate value was required since this affects the pipe size and respective insulation thickness. As per typical PEM installations on the kW scale,⁴¹ a flow rate of 8 ml s⁻¹ cm⁻² relative to the size of the MEA was assumed. A total MEA size of 1 m² hence equalled a flow rate of 0.08 m³ s⁻¹. A pipe diameter was chosen such that the fluid velocity does not exceed 2.5 m s⁻¹ in the pipework. For the temperature in question and calculated pipe diameter, ASHRAE standards³⁸ suggest an insulation thickness of 0.08 m (for an insulation thermal conductivity of 0.039 W m⁻¹ K⁻¹). The entire pipework is assumed to have a total length of 10 m.

Results and Discussion

Following the approach described above, the ET-PEMWE system is modelled to utilise energy in the most efficient manner possible, in that heat energy from the irreversible losses is used to heat the feed water dosed to the system and if available, for secondary heating purposes.

Figure 4 displays this energy transfer process assuming no heat losses from the stack and pipework whilst Fig. 5 does take into account these losses in the system. Starting with the former case, \dot{Q}_{heat,H_2O} increases linearly with higher current densities as more feed water is required to make up for the consumed water. As given by the inset, \dot{Q}_{stack} is positive (*Case 1*) until approximately 0.24 A cm⁻². Above this point, heat from the irreversible losses is sufficient to sustain the $T\Delta S$ energy component and any excess can be used to heat the feed water (*Case 3A*), hence reducing the load on \dot{Q}_{heat,H_2O} . This energy recovery is signified with \dot{Q}'_{heat,H_2O} , so when this quantity becomes zero, no additional energy is needed to heat the additional water to balance the consumed water of the electrolysis reaction. For the considered scenario, no feed water heating is required above approximately 0.52 A cm⁻² (where \dot{Q}'_{heat,H_2O} is

Table I. Key Equations for the computation of energy and exergy efficiency in ET-PEMWE (with or without the consideration for heat losses).

$$\dot{Q}_j = iA_{MEA}(U - U_{rev})$$

$$\dot{N}_{H_2,out} = \frac{iA_{MEA}}{2F} = \dot{N}_{H_2O,react}$$

$$e\dot{Q}_{heat,H_2O} = \dot{Q}_{theo,heat,H_2O}$$

$$\dot{Q}_{heat,H_2O,rec} = |\dot{Q}_{stack}| \left(1 - \frac{T_0}{T}\right) \frac{T_s}{(T_s - T_0)}$$

$$\dot{Q}'_{heat,H_2O} = \dot{Q}_{heat,H_2O} - |\dot{Q}_{stack}| \left(1 - \frac{T_0}{T}\right) \left(\frac{T_s}{T_s - T_0}\right)$$

$$\dot{Q}_{stack,heat} = \dot{Q}_{heat,H_2O} \left(1 - \frac{T_0}{T_s}\right) \frac{T}{(T - T_0)}$$

$$\dot{Q}_{stack,rec} = |\dot{Q}_{stack}| - \dot{Q}_{stack,heat}$$

In the case where no heat losses are considered

$$\dot{Q}_{stack} = (\dot{Q}_{react} - \dot{Q}_j)$$

$$\dot{Q}_{theo,heat,H_2O} = \frac{iA_{MEA}}{2F} (H_{H_2O}^T - H_{H_2O}^{T_0})$$

In the case where heat losses in the stack and pipework are considered

$$\dot{Q}_{stack} = (\dot{Q}_{react} + \dot{Q}_{loss,stack} - \dot{Q}_j)$$

$$\dot{Q}_{theo,heat,H_2O} = \frac{iA_{MEA}}{2F} (H_{H_2O}^T - H_{H_2O}^{T_0}) + \dot{Q}_{loss,pipe}$$

Table II. Relevant efficiencies for the different possible heat management cases.

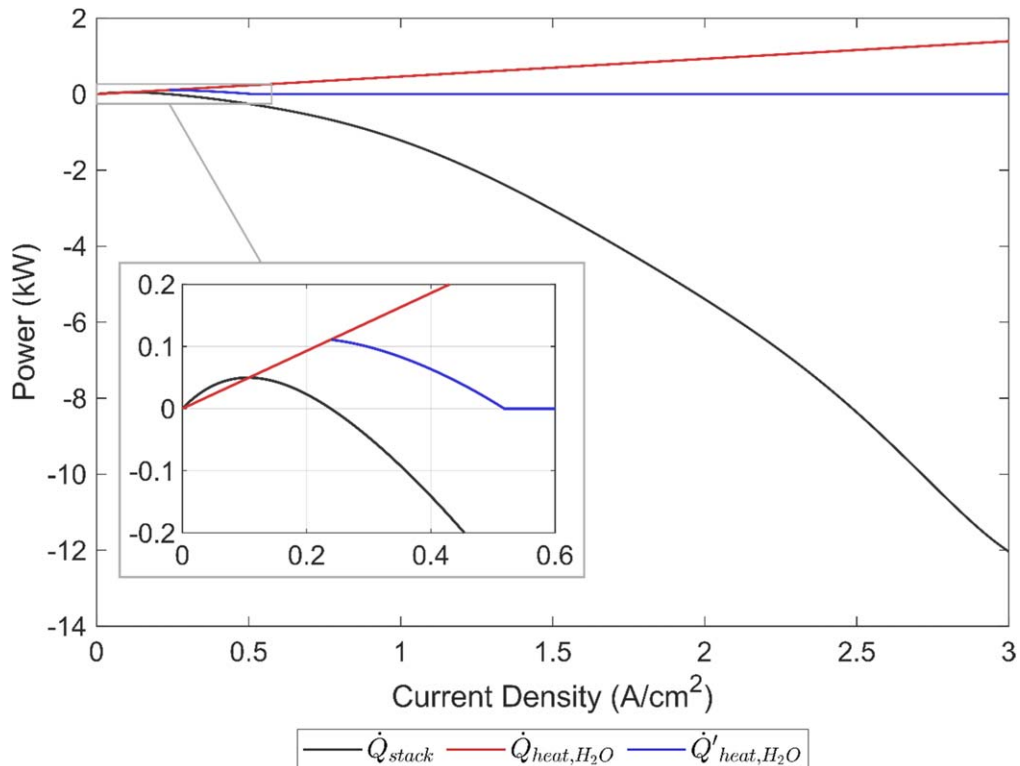
Case	Determination of Energy and Exergy Efficiency
1: $\dot{Q}_{stack} > 0$	$\eta_{en} = \frac{LHV_{H_2} \dot{N}_{H_2, out}}{P_{electric} + \dot{Q}_{stack} + \dot{Q}_{heat, H_2O}}$ $\eta_{ex} = \frac{E_{H_2} \dot{N}_{H_2, out}}{P_{electric} + \dot{Q}_{stack} \left(1 - \frac{T_0}{T_s}\right) + \dot{Q}_{heat, H_2O} \left(1 - \frac{T_0}{T_s}\right)}$
2: $\dot{Q}_{stack} = 0$	$\eta_{en} = \frac{LHV_{H_2} \dot{N}_{H_2, out}}{P_{electric} + \dot{Q}_{heat, H_2O}}$ $\eta_{ex} = \frac{E_{H_2} \dot{N}_{H_2, out}}{P_{electric} + \dot{Q}_{heat, H_2O} \left(1 - \frac{T_0}{T_s}\right)}$
3A: $\dot{Q}_{stack} < 0$	$\eta_{en} = \frac{LHV_{H_2} \dot{N}_{H_2, out}}{P_{electric} + \left(\dot{Q}_{heat, H_2O} - \dot{Q}_{stack} \left(1 - \frac{T_0}{T_s}\right) \left(\frac{T_s}{T_s - T_0}\right)\right)}$ $\eta_{ex} = \frac{E_{H_2} \dot{N}_{H_2, out}}{P_{electric} + \left(\dot{Q}_{heat, H_2O} - \dot{Q}_{stack} \left(1 - \frac{T_0}{T_s}\right) \left(\frac{T_s}{T_s - T_0}\right)\right) \left(1 - \frac{T_0}{T_s}\right)}$
3B: $\dot{Q}_{stack} < 0$ Heat in excess to that required in the system	$\eta_{en} = \frac{LHV_{H_2} \dot{N}_{H_2, out} + \dot{Q}_{stack, rec}}{P_{electric}}$ $\eta_{ex} = \frac{E_{H_2} \dot{N}_{H_2, out} + \dot{Q}_{stack, rec} \left(1 - \frac{T_0}{T_s}\right)}{P_{electric}}$

Table III. Key operating parameters.

T_{stack} (K)	p (bar)	T_s (K)	T_e (K)
393	3 (abs)	413	298

driven to zero) as this is being entirely supplied by the irreversible losses, giving rise to *Case 3B*. (\dot{Q}_{heat, H_2O} is still displayed throughout the entire current density range so as to show the energy recovery potential for feed water heating).

A similar pattern is observed in Fig. 5, which accounts for stack and pipework heat losses. In this case, the threshold for full internal heat integration is shifted towards a higher current density. Additional heat must be provided to the stack until approximately 1.08 A cm^{-2} to sustain the electrochemical reaction whilst from a current density of approximately 1.44 A cm^{-2} , the excess energy is capable of satisfying the entire feed water heating demand. Fig. 5 does not show the recoverable thermal power in *Case 3B*. In this regard, Fig. 6 displays the share of power throughout the entire current density range. The green area, identified as $P_{electric, rev}$ in the plot, shows the minimum electrical power required for the reaction


Figure 4. Thermal energy transfer when no heat losses are considered.

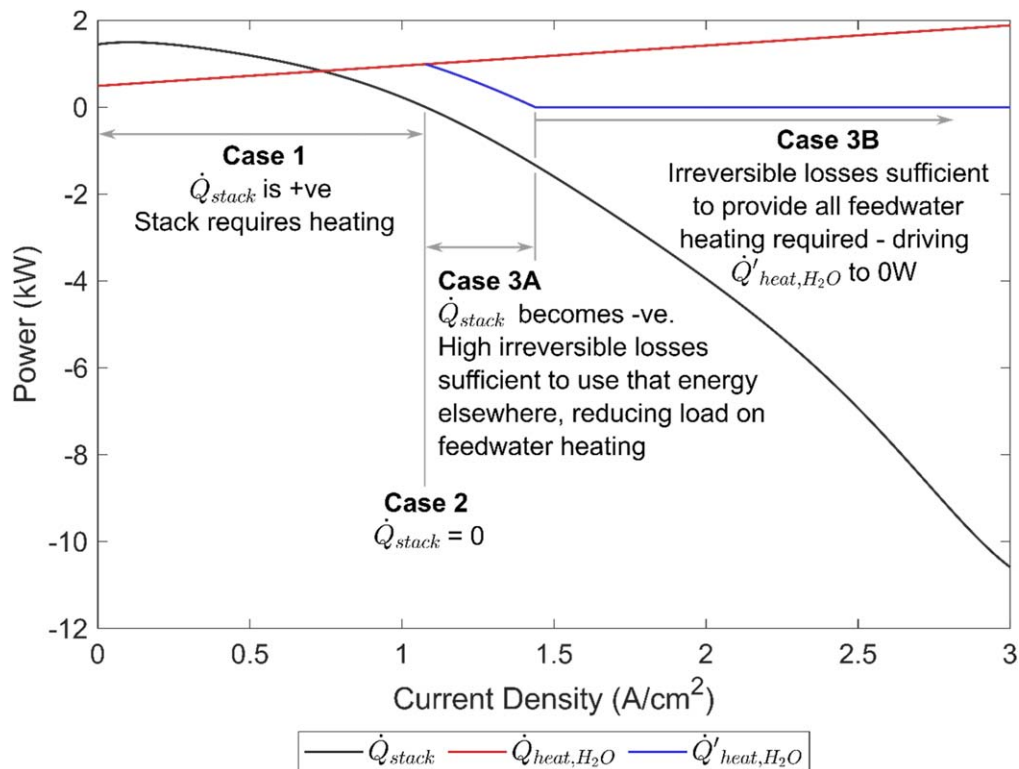


Figure 5. Thermal energy transfer when accounting for heat losses in the stack and pipework.

to occur to provide for $\Delta G_{rev}(T, p)$ whilst the yellow area shows the fraction of irreversible losses. Heating inputs to the stack and feed water become progressively unnecessary as polarization losses make up for these heating requirements. Their values in the plot are reduced to 0 W at the current densities outlined in the text above. The red part also arises from $P_{electric}$ but is the fraction of power which can potentially be recovered for additional heating applications.

Exergy efficiency for ET-PEMWE.—Figure 7 presents the resulting exergy efficiencies for ET-PEMWE. The advantage of presenting the exergy efficiency lies in the consideration of having different forms of energy within a system. When heat losses are considered, efficiency starts from very low values. At low current densities, a substantial amount of energy is simply utilised to compensate heat losses in the pipework and stack. The efficiency difference between the two curves becomes progressively smaller with increasing current density. This region coincides with *Case 3B* where all electrical power becomes utilised in some manner and the only difference between the two curves solely results from the stack and pipework losses which lower the amount of thermal power which can be recovered ($\dot{Q}_{stack,rec}$). This constitutes only a minor fraction of total power share and its effect decreases with a higher $P_{electric}$ input to the stack.

Effect of no heat recovery.—For this step, the model was adapted such that no heat recovery takes place—the heat originating from the irreversible losses would not be used to heat the feed water or recovered for secondary heating but simply dissipated into the surrounding. The model hence followed only two cases—*Case 1* when $\dot{Q}_{stack} > 0$ and *Case 2* once $\dot{Q}_{stack} \leq 0$.

As shown in Fig. 8, *Case 1* remains unchanged since the irreversible losses would still provide a heat source to the $T\Delta S$ energy component. Once $\dot{Q}_{stack} \leq 0$ and the current density increases, the efficiency drops to lower values than when an energy recovery strategy is in place, reaching a maximum efficiency drop of 4.2%

points at 3 A cm^{-2} . This trend can be attributed to a decreasing fraction of recovered energy with respect to electrical power input.

Comparison to LT PEMWE.—Improved performance at higher temperatures is often considered as a key advantage for opting for ET-PEMWE over LT. In order to compare the performance which can be obtained by the two operating regimes, the model was adapted for the LT scenario using polarization curve data at $80 \text{ }^\circ\text{C}$ for the same membrane thickness, also extracted from the study by Garbe et al.⁴⁰ This allows a comparison based on results from the same WE setup.

Figure 9 compares the thermodynamic parameters outlined in Eq. 1 involving the electrochemical reaction for water electrolysis. Changes mainly occur in ΔG_{stack} and $T\Delta S$. Higher temperatures allow a lower Gibbs free energy which translates to a lower reversible potential for hydrogen production. On the contrary, more heat input is needed to provide for the $T\Delta S$ term.

Figures 10 and 11 respectively display the exergy and energy efficiencies obtained for ET and LT operation. At low current densities, the higher heating requirements for ET cause the exergy efficiency to be lower than at LT. The ET efficiency however improves to the point where it surpasses that for LT at around 0.54 A cm^{-2} . This can be attributed to (i) a lower electrical power input for the same production of hydrogen (as shown in the polarization curve data in Fig. 12) and (ii) energy recovery which reduces the load on the required heat inputs. The latter point is more clear when re-visiting the results in Fig. 8.

The efficiency difference is accentuated with increasing current density, reaching 3.8 % points at 3 A cm^{-2} . Indeed, the slightly different gradients of the polarization curves in Fig. 12 show that the LT calls for an increasing requirement of electrical power input (compared to ET). Moreover, the higher temperature difference adds more value to the recovered heat, as taken into consideration by the application of $(1 - T_0/T)$, referred to as the *exergetic temperature factor* by Dincer and Rosen.³⁴

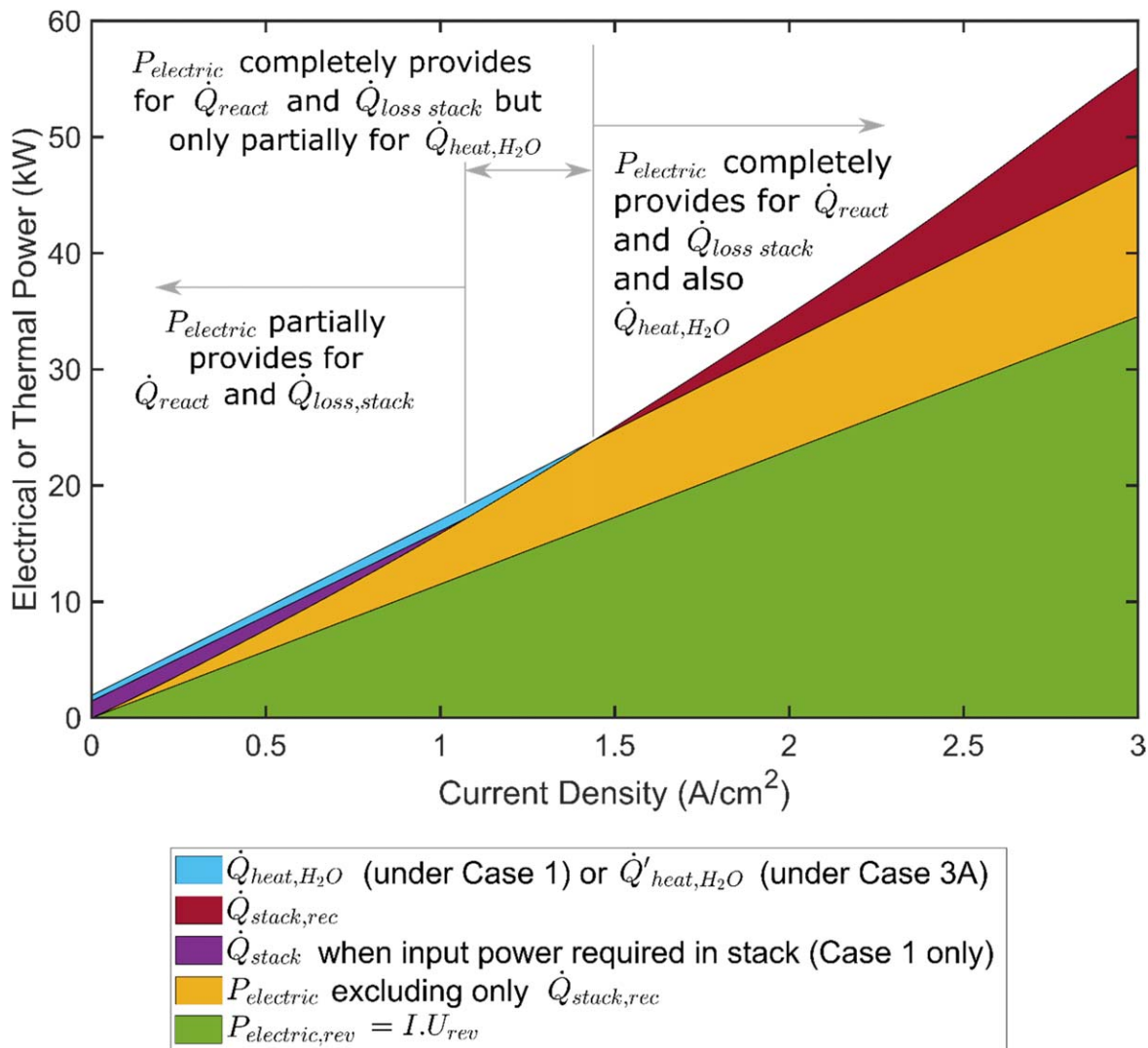


Figure 6. Thermal and electrical power share.

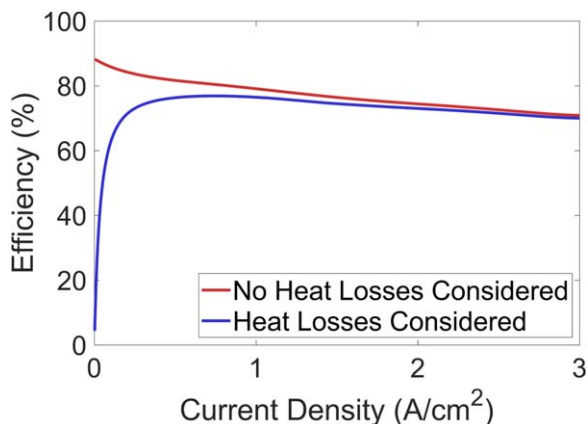


Figure 7. Exergy efficiency for the ET-PEMWE model.

It turns out that application of this factor outweighs the effect of higher $\dot{Q}_{stack,rec}$ in the LT case when computing the exergy efficiency. The higher $\dot{Q}_{stack,rec}$ can be explained from Fig. 13, displaying $|\dot{Q}_{stack}|$ and $\dot{Q}_{stack,heat}$ with the latter providing for the internal system heat requirements. The difference between the two

curves (for the same temperature) corresponds to the thermal power which could potentially be recovered for secondary applications. More thermal power is made available for the LT due to the higher polarization losses. However, application of the exergetic temperature factor in the exergy efficiency equation adds more weight to that recovered by the ET. The penalty incurred with utilising lower temperatures sheds light on the suitability of exergy efficiency as a performance indicator for PEMWE systems.

This trend is indeed not captured when computing the energy efficiency, shown in Fig. 11. LT is favoured throughout the entire current density range. The efficiency difference does reduce towards $1 A cm^{-2}$ as the effect of thermal power inputs is reduced and the efficiency becomes more a function of electrical power (hence favouring ET). However, triggering Case 3B, identified by the sudden change in gradient at $1 A cm^{-2}$ (for the LT curve), causes an abrupt increase in efficiency as a portion of supplied electrical power is utilised as $\dot{Q}_{stack,rec}$ (in the numerator of Eq. 35). Given that LT is characterised by larger losses (resulting in more $\dot{Q}_{stack,rec}$) and that no distinction is made with respect to temperature difference, its energy efficiency increases more than for the ET system.

Nonetheless, both curves show a similar trend of improved energy efficiency with increasing current density. It is hence expected that heat recovery would make (both LT and ET) PEMWE systems more favourable even at higher current densities.

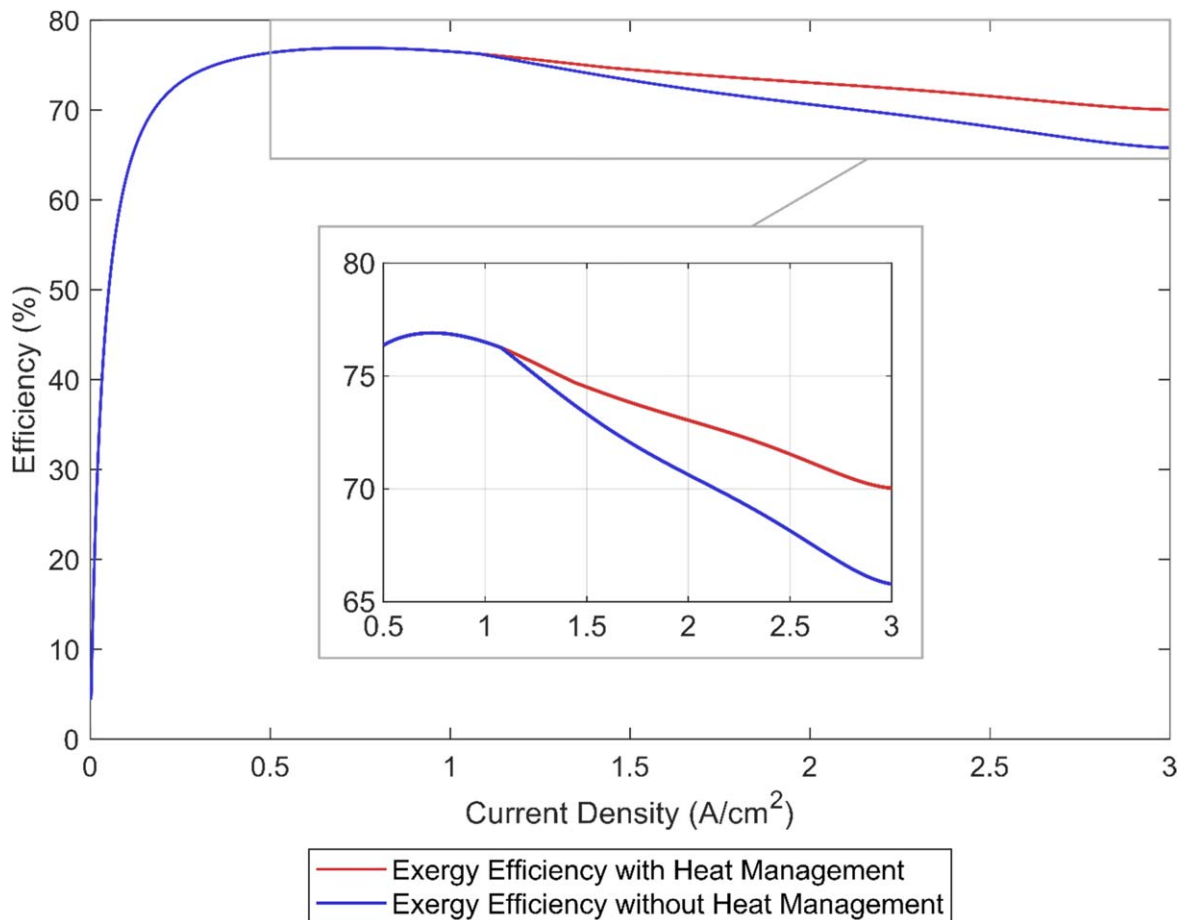


Figure 8. Effect on exergy efficiency when no energy recovery occurs.

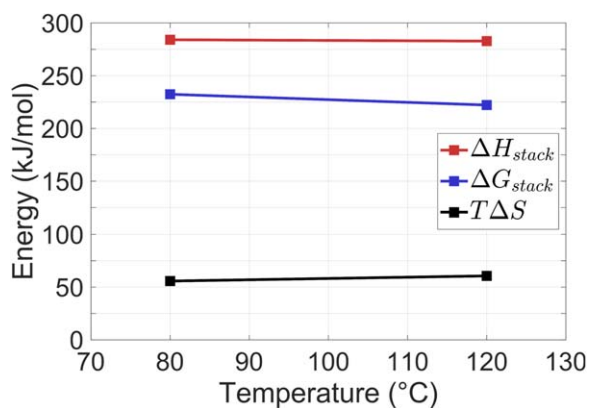


Figure 9. Comparison of ET and LT thermodynamic parameters.

Effect of higher heat losses.—The model is based on a multitude of parameters, each of which has been assigned so as to best represent a realistic simulation. Nonetheless, the possible variability in the input variables would have an effect on the calculated efficiencies. In order to assess to what extent the target variable is affected, the model was re-run with a different value for pipework length—from 10 m (in the original model) to 40 m, expected to simulate higher heat losses. This is hereunder referred to as “Enhanced Heat Loss.”

The effect on exergy efficiency can be seen in Fig. 14, with the greatest difference (when compared to the original data) occurring in the lower current density region and equalling 12.2 % points. This difference decreases with increasing current density as the heat

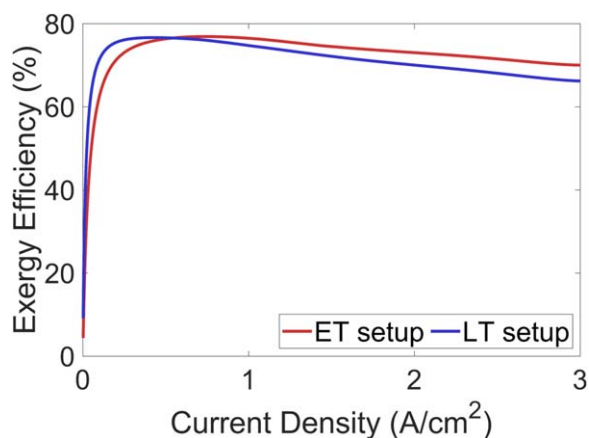


Figure 10. Exergy efficiency comparison to LT PEMWE.

losses become a much smaller share of total power involved, reaching 0.7 % points at 3 A cm⁻².

Model simplifications.—A number of measures were included in the model to best simulate the ET system such as the use of an effectiveness factor (ϵ) for heat exchangers, taking into account heat losses from the pipework and stack and analysing the effect of the “Enhanced Heat Loss” case.

On the other hand, one of the simplifications in the model involved the energy within the exiting hot gas streams not being recovered. In order to quantify the effect of not doing so, the maximum energy which could be potentially recovered was

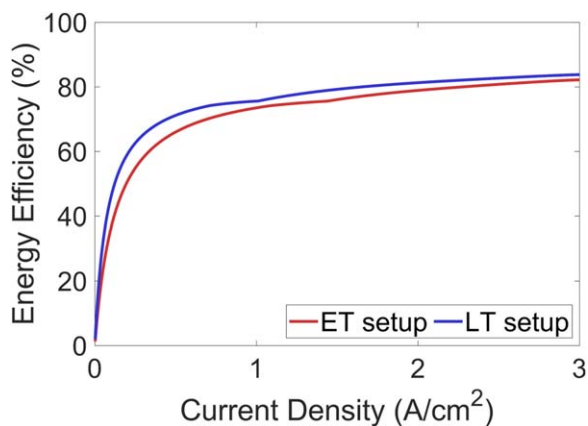


Figure 11. Energy efficiency comparison to LT PEMWE.

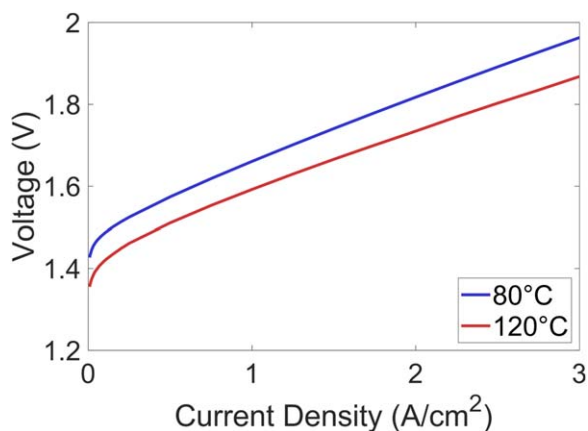


Figure 12. Polarization curves for ET and LT as adopted in the model, with permission from Ref. 40.

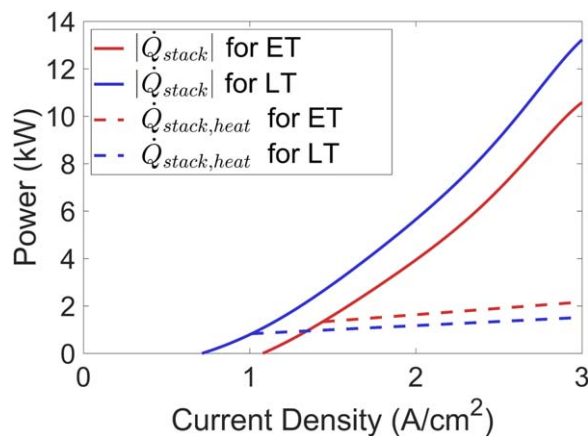


Figure 13. Extent of recovered heat with ET and LT systems.

calculated by assuming these would be cooled from 393 K down to room temperature at 298 K.

Based on the gas production at 3 A cm^{-2} , this recovery was calculated to collectively amount to approximately 650W. This constitutes around 7.7 % of the energy recovered from the stack ($\dot{Q}_{stack,rec}$). Acknowledging this quantity is not appreciably significant, these gases would in any case require cooling to remove any moisture carry-over and hence purify the produced gases. Such a step should hence not be discounted in the design of ET systems.

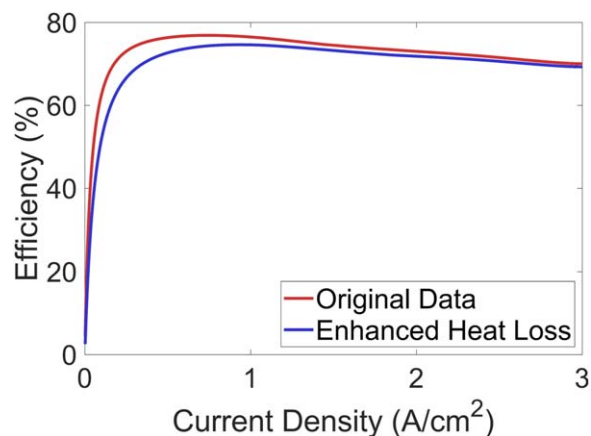


Figure 14. Effect of higher heat losses on exergy efficiency.

Further considerations.—This study considers an ET-PEMWE system from an efficiency standpoint. To do so, it assumes that all hardware and stack components can operate reliably over the intended lifetime. Nonetheless, ET-PEMWE is still an emerging technology and this section is hence intended to briefly outline the current limitations with respect to the system considered in the model. It also presents a number of factors which would need to be considered for a cost-effective implementation of such systems.

Device durability.—Degradation studies have not yet been performed in the timescales employed for LT and a noticeable decline in performance within the first 400 h of operation has always been observed for ET.^{2,10,42} Multiple degradation mechanisms may be in play, with membrane thinning and titanium passivation being significant contributors with increasing temperatures.⁴³ Titanium passivation has been specifically tackled at ET with the application of coatings such as IrO_2 -coated Ti mesh for the oxygen electrode.⁴² In the case of phosphoric acid based (steam) systems, tantalum was found as a highly corrosion resistant construction material.⁶ It follows that such coatings have a direct impact on investment costs.

Operational considerations.—Water electrolyzers employ ion exchangers for water purification within the circuit. Typically, these do not withstand temperatures higher than 80°C . Accommodating this limitation would entail cooling the liquid water to a suitable range (ideally, re-using the transferred heat) and heating it back to the operating temperature after the ion exchanger. When the model was re-run with the chosen flow rate, based on that typically used on the industrial scale at 60°C , the heat energy bill (to raise the temperature from 80°C to 120°C) was found to be excessively high to be provided by the recovered heat from the stack. In reality, much lower flow rates may be possible without running into mass transfer problems within the stack and the choice of flow rate hence becomes a determining parameter in ET conditions. Alternatively, a by-pass purification system may be set up where only a part of the circulated water (1/10th for instance) is sent to a cooler and then through purification, strongly reducing the required energy. Efforts to devise water purification techniques suitable for ET-PEMWE would also simplify this issue.

Further to model limitations, the system is considered to be brought to the operating temperature and then allowed to run continuously. No start-ups or shutdowns are hence taken into account. In reality, their frequency would exert an influence on the additional heat energy bill which must be paid for ET operation.

It would also be expected that a higher temperature setup would necessitate more control and safety requirements. Moreover, installed hardware (such as fittings) would need to withstand the more challenging operating conditions and would call for a higher Capital and Operational Expenditure (CAPEX and OPEX).

More development is hence required in ET systems to reap the benefits of improved efficiency, with a techno-economic analysis bringing into picture the operating cost reductions (due to better efficiency) and the total expenditure of the system.

Conclusions

An energy and exergy analysis has been performed to evaluate the performance of ET-PEMWE, with the model aiming to utilise the energy in the most efficient manner and also take into account potential thermal losses.

The stack operates in autothermic mode for a considerable range of current densities. Heating inputs to the stack and feed water become progressively unnecessary as polarization losses make up for these heating requirements. For the considered model, a current density above 1.44 A cm^{-2} would allow surplus heat to be utilised for secondary applications such as district heating but not recovering any heat would result in an exergy efficiency loss of 4.2 % points (at the maximum considered current density).

The exergy efficiency for ET has been calculated to surpass that for LT at 0.54 A cm^{-2} . This improvement is attributed to (i) a lower electrical power input for the same production of hydrogen and (ii) energy recovery. The maximum registered improvement reaches 3.8 % points at 3 A cm^{-2} . The exergetic temperature factor favours higher temperature differences—a benefit which outweighs the fact that a greater quantity of thermal power is recovered in the LT system (due to higher polarization losses).

This finding also shows the suitability of adopting exergy efficiency as a performance indicator in PEMWE systems. Energy efficiency does not capture the effect of temperature differences, resulting in the LT exhibiting a higher efficiency throughout the entire current density range.

The model does not account for the use of steam, which is another alternative (to liquid water) when operating with ET-PEMWE. Phosphoric acid doped PFSA membranes have been predominantly studied for steam-based systems.^{3,6-8} As pointed out by Jensen et al.,⁴⁴ these are in such case not operated at the optimum humidification as when flooded with water, resulting in a drop in membrane conductivity which directly influences the ohmic overpotential. The higher voltage requirements with respect to liquid operation (evidenced by polarization curves in Jensen et al.⁴⁴) would hence be expected to decrease efficiency. Furthermore, cooling may be required for easier transport of liquid water, necessitating further heat exchangers and hence incurring further efficiency losses. Nonetheless, possible future improvements in the membranes' performance for steam operation would then make such an analysis worth re-visiting.

This work has furthered the understanding on the performance of ET-PEMWE and evaluated the cost borne with opting for more

demanding higher temperature conditions from the perspective of energy and exergy efficiency.

Acknowledgments

We thank Lorenz Gubler and Steffen Garbe for kindly providing us with the polarization curve data and granting us permission to use it in the model.

Appendix

This section details the approach to calculate the Gibbs free energy change for non-standard pressure and conditions, and departs from Eqs. 8 and 9 in the text above, hereunder reproduced as A.1 and A.2:

$$\Delta G_{rev}(T, p) = \Delta G_{rev}^*(T) + RT \ln \left(\frac{a_{H_2} a_{O_2}^{1/2}}{a_{H_2O}} \right) \quad [A.1]$$

Where:

$$a_i = \frac{f_i}{p_{ref}} \quad [A.2]$$

Fugacity (f_i) is used to account for the deviation of the system from ideal gas behaviour:³¹

$$f_i = \phi_i p_i \quad [A.3]$$

Where ϕ_i is the fugacity coefficient of a pure gas i and can be derived from the second virial coefficient (B_i) obtained from data tables⁴⁵ such that:

$$\ln(\phi_i) = \frac{B_i p_i}{RT} \quad [A.4]$$

In the case of the partial pressures p_i , these are computed from the total anode/cathode chamber pressure and the saturation vapour pressure of water ($p_{H_2O,sat}$) at the respective temperature, such that:⁴⁶

$$p_{O_2} = p_{an} - p_{H_2O,sat} \quad [A.5]$$

$$p_{H_2} = p_{cat} - p_{H_2O,sat} \quad [A.6]$$

Where the saturated vapour pressure of water ($p_{H_2O,sat}$) is given by the Antoine equation:⁴⁷

Table A-I. Parameters for Eq. A.7.⁴⁵






For $1 \text{ }^\circ\text{C} \leq T_{celsius} \leq 100 \text{ }^\circ\text{C}$			For $99 \text{ }^\circ\text{C} \leq T_{celsius} \leq 374 \text{ }^\circ\text{C}$		
A	B	C	A	B	C
8.07131	1730.63	233.426	8.14019	1810.94	244.485

$$p_{\text{H}_2\text{O},\text{sat}} = 10^{A - \frac{B}{C + T_{\text{celsius}}}} \quad [\text{A}\cdot 7]$$

Where T_{celsius} refers to the temperature (in °C) and A , B , C are constants based on the temperature of interest, as per Table A-I.

A similar approach is used at the cathode for the computation of the partial pressure of hydrogen.

ORCID

Marco Bonanno  <https://orcid.org/0000-0002-4324-6313>
 Karsten Müller  <https://orcid.org/0000-0002-7205-1953>
 Boris Benschmann  <https://orcid.org/0000-0001-8685-7192>
 Richard Hanke-Rauschenbach  <https://orcid.org/0000-0002-1958-307X>
 Retha Peach  <https://orcid.org/0000-0001-7697-0781>
 Simon Thiele  <https://orcid.org/0000-0002-4248-2752>

References

1. A. Valente, D. Iribarren, and J. Dufour, "Cumulative Energy Demand of Hydrogen Energy Systems." *Energy Footprints of the Energy Sector*, ed. S. S. Muthu (Springer, Singapore) 48 (2019).
2. J. Mališ, P. Mazúr, M. Paidar, T. Bystron, and K. Bouzek, "Nafion 117 stability under conditions of PEM water electrolysis at elevated temperature and pressure." *Int. J. Hydrogen Energy*, **41**, 2177 (2016).
3. D. Aili, M. K. Hansen, C. Pa, Q. Li, E. Christensen, J. O. Jensen, and N. J. Bjerrum, "Phosphoric acid doped membranes based on Nafion®, PBI and their blends—Membrane preparation, characterization and steam electrolysis testing." *Int. J. Hydrogen Energy*, **36**, 6985 (2011).
4. U. Babic, M. Suermann, F. N. Büchi, L. Gubler, and T. J. Schmidt, "Review-identifying critical gaps for polymer electrolyte water electrolysis development." *J. Electrochem. Soc.*, **164**, F387 (2017).
5. H. Li, T. Fujigaya, H. Nakajima, A. Inada, and K. Ito, "Optimum structural properties for an anode current collector used in a polymer electrolyte membrane water electrolyzer operated at the boiling point of water." *J. Power Sources*, **332**, 16 (2016).
6. M. K. Hansen, D. Aili, E. Christensen, C. Pan, S. Eriksen, J. O. Jensen, J. H. von Barner, Q. Li, and N. J. Bjerrum, "PEM steam electrolysis at 130 °C using a phosphoric acid doped short side chain PFSA membrane." *Int. J. Hydrogen Energy*, **37**, 10992 (2012).
7. J. Xu, Q. Li, M. K. Hansen, E. Christensen, A. L. Tomás García, G. Liu, X. Wang, and N. J. Bjerrum, "Antimony doped tin oxides and their composites with tin pyrophosphates as catalyst supports for oxygen evolution reaction in proton exchange membrane water electrolysis." *Int. J. Hydrogen Energy*, **37**, 18629 (2012).
8. J. Xu, D. Aili, Q. Li, E. Christensen, J. O. Jensen, W. Zhang, M. K. Hansen, G. Liu, X. Wang, and N. J. Bjerrum, "Oxygen evolution catalysts on supports with a 3-D ordered array structure and intrinsic proton conductivity for proton exchange membrane steam electrolysis." *Energy Environ. Sci.*, **7**, 820 (2014).
9. H. Li, A. Inada, T. Fujigaya, H. Nakajima, K. Sasaki, and K. Ito, "Effects of operating conditions on performance of high-temperature polymer electrolyte water electrolyzer." *J. Power Sources*, **318**, 192 (2016).
10. V. Antonucci, A. Di Blasi, V. Baglio, R. Ornelas, F. Matteucci, J. Ledesma-Garcia, L. G. Arriaga, and A. S. Aricò, "High temperature operation of a composite membrane-based solid polymer electrolyte water electrolyser." *Electrochim. Acta*, **53**, 7350 (2008).
11. V. Baglio, R. Ornelas, F. Matteucci, F. Martina, G. Ciccarella, I. Zama, L. G. Arriaga, V. Antonucci, and A. S. Aricò, "Solid polymer electrolyte water electrolyser based on nafion-TiO₂ composite membrane for high temperature operation." *Fuel Cells*, **9**, 247 (2009).
12. W. Xu, K. Scott, and S. Basu, "Performance of a high temperature polymer electrolyte membrane water electrolyser." *J. Power Sources*, **196**, 8918 (2011).
13. P. Mazúr, J. Polonský, M. Paidar, and K. Bouzek, "Non-conductive TiO₂ as the anode catalyst support for PEM water electrolysis." *Int. J. Hydrogen Energy*, **37**, 12081 (2012).
14. A. Skulimowska, M. Dupont, M. Zaton, S. Sunde, L. Merlo, D. J. Jones, and J. Rozière, "Proton exchange membrane water electrolysis with short-side-chain Aquion® membrane and IrO₂ anode catalyst." *Int. J. Hydrogen Energy*, **39**, 6307 (2014).
15. J. Polonský, P. Mazúr, M. Paidar, E. Christensen, and K. Bouzek, "Performance of a PEM water electrolyser using a TaC-supported iridium oxide electrocatalyst." *Int. J. Hydrogen Energy*, **39**, 3072 (2014).
16. P. Olivier, C. Bourasseau, and P. B. Bouamama, "Low-temperature electrolysis system modelling: A review." *Renew. Sustain. Energy Rev.*, **78**, 280 (2017).
17. P. Ahmadi, I. Dincer, and M. A. Rosen, "Thermodynamic modeling and multi-objective evolutionary-based optimization of a new multigeneration energy system." *Energy Convers. Manage.*, **76**, 282 (2013).
18. P. Ahmadi, I. Dincer, and M. A. Rosen, "Energy and exergy analyses of hydrogen production via solar-boosted ocean thermal energy conversion and PEM electrolysis." *Int. J. Hydrogen Energy*, **38**, 1795 (2013).
19. M. Calderón, A. J. Calderón, A. Ramiro, J. F. González, and I. González, "Evaluation of a hybrid photovoltaic-wind system with hydrogen storage performance using exergy analysis." *Int. J. Hydrogen Energy*, **36**, 5751 (2011).
20. B. Laoun, A. Khellaf, M. W. Naceur, and A. M. Kannan, "Modeling of solar photovoltaic-polymer electrolyte membrane electrolyzer direct coupling for hydrogen generation." *Int. J. Hydrogen Energy*, **41**, 10120 (2016).
21. F. Moradi Nafchi, E. Baniasadi, E. Afshari, and N. Javani, "Performance assessment of a solar hydrogen and electricity production plant using high temperature PEM electrolyzer and energy storage." *Int. J. Hydrogen Energy*, **43**, 5820 (2018).
22. H. Nami and E. Akrami, "Analysis of a gas turbine based hybrid system by utilizing energy, exergy and exergoeconomic methodologies for steam, power and hydrogen production." *Energy Convers. Manage.*, **143**, 326 (2017).
23. Y. E. Yuksel, M. Ozturk, and I. Dincer, "Thermodynamic performance assessment of a novel environmentally-benign solar energy based integrated system." *Energy Convers. Manage.*, **119**, 109 (2016).
24. H. Zhang, S. Su, G. Lin, and J. Chen, "Efficiency calculation and configuration design of a PEM electrolyser system for hydrogen production." *Int. J. Electrochem. Sci.*, **7**, 4143 (2012).
25. M. Ni, M. K. H. Leung, and D. Y. C. Leung, "Energy and exergy analysis of hydrogen production by a proton exchange membrane (PEM) electrolyzer plant." *Energy Convers. Manage.*, **49**, 2748 (2008).
26. M. Ni, M. K. H. Leung, and D. Y. C. Leung, "Energy and exergy analysis of hydrogen production by solid oxide steam electrolyzer plant." *Int. J. Hydrogen Energy*, **32**, 4648 (2007).
27. H. Zhang, S. Su, G. Lin, and J. Chen, "Evaluation and calculation on the efficiency of a water electrolysis system for hydrogen production." *Int. J. Hydrogen Energy*, **35**, 10851 (2010).
28. R. P. O'Hayre, S. Cha, W. G. Colella, and F. B. Prinz, *Fuel Cell Fundamentals* (Wiley, Hoboken, NJ) 3rd ed. (2016).
29. National Institute of Standards and Technology, (2021), Chemistry Webbook U.S. Department of Commerce. Available at <https://webbook.nist.gov/chemistry/form-ser/>.
30. L. Zachert, M. Suermann, B. Benschmann, and R. Hanke-Rauschenbach, "Energetic evaluation and optimization of hydrogen generation and compression pathways considering PEM water electrolyzers and electrochemical hydrogen compressors." *J. Electrochem. Soc.*, **168**, 14504 (2021).
31. I. Tosun, *The Thermodynamics of Phase and Reaction Equilibria* (Elsevier, Amsterdam; Oxford, UK) 1st ed. (2013).
32. W. J. Tjittak, *Thesis*, TU Delft, The Netherlands (2019).
33. A. F. Mills and C. F. M. Coimbra, *Basic Heat and Mass Transfer* (Temporal Publishing, San Diego, CA) 3rd ed. (2015).
34. I. Dincer and M. Rosen, *Exergy: Energy, Environment and Sustainable Development* (Elsevier, Amsterdam; Oxford, UK) 2nd ed. (2013).
35. N. Sato, *Chemical Energy and Exergy: An Introduction to Chemical Thermodynamics for Engineers* (Elsevier, Amsterdam, The Netherlands) 1st ed. (2004).
36. *Energetische Arbeitsmappe* (Springer, Heidelberg, Germany) 15th ed. (2000).
37. F. P. Incropera, D. P. Dewitt, T. L. Bergman, and A. S. Lavine, *Fundamentals of Heat and mass transfer* (Wiley, Hoboken, NJ) 6th ed. (2007).
38. ASHRAE, *Standard 90.1-2007—Energy Standard for Buildings Except Low-Rise Residential Buildings* (2007), <https://www.ashrae.org/technical-resources/standards-and-guidelines/standards-addenda/addenda-to-standard-90-1-2007-ip-and-si-versions>.
39. H. Zhang, S. Su, X. Chen, G. Lin, and J. Chen, "Performance evaluation and optimum design strategies of an acid water electrolyzer system for hydrogen production." *Int. J. Hydrogen Energy*, **37**, 18615 (2012).
40. S. Garbe, J. Futter, T. J. Schmidt, and L. Gubler, "Insight into elevated temperature and thin membrane application for high efficiency in polymer electrolyte water electrolysis." *Electrochim. Acta*, **377**, 138046 (2021).
41. M. Espinosa-López, C. Darras, P. Poggi, R. Glises, P. Baucour, A. Rakotondrainibe, S. Besse, and P. Serre-Combe, "Modelling and experimental validation of a 46 kW PEM high pressure water electrolyzer." *Renewable Energy*, **119**, 160 (2018).
42. S. Choe, B. Lee, M. K. Cho, H. Kim, D. Henkensmeier, S. J. Yoo, J. Y. Kim, S. Y. Lee, H. S. Park, and J. H. Jang, "Electrodeposited IrO₂/Ti electrodes as durable and cost-effective anodes in high-temperature polymer-membrane-electrolyte water electrolyzers." *Appl. Catalysis B*, **226**, 289 (2018).
43. S. H. Frensch, F. Fouda-Onana, G. Serre, D. Thoby, S. S. Araya, and S. Kær, "Influence of the operation mode on PEM water electrolysis degradation." *Int. J. Hydrogen Energy*, **44**, 29889 (2019).
44. J. O. Jensen, C. Chatzichristodoulou, E. Christensen, N. J. Bjerrum, and W. Li, "Intermediate temperature electrolyzers." *Electrochemical Methods for Hydrogen Production*, ed. K. Scott (Royal Society of Chemistry, UK) 253 (2019).
45. J. M. H. Levelt Sengers, M. Klein, and J. Gallagher, *Pressure-Volume-Temperature Relationships of Gases Virial Coefficients*. (National Bureau of Standards, Washington DC, USA) (1971).
46. V. Liso, G. G. Savoia, S. S. Araya, G. Cinti, and S. K. Kær, "Modelling and experimental analysis of a polymer electrolyte membrane water electrolysis cell at different operating temperatures." *Energies*, **11**, 3273 (2018).
47. Dortmund Data Bank GmbH, *Saturated Liquid Density DDB* (2020), Available at <http://ddbonline.ddb-st.de/AntoineCalculation/AntoineCalculationCGI.exe?component=Water>.